A ''modified Lennard-Jones oscillator'' model for diatom potential functions

Photos G. Hajigeorgiou[a] and Robert J. Le Roy[b]
Guelph-Waterloo Centre for Graduate Work in Chemistry and Biochemistry, University of Waterloo, Waterloo, Ontario N2L 3G1, Canada

(Received 27 August 1999; accepted 8 December 1999)

A flexible new analytical representation for the internuclear potential energy of a diatomic molecule is proposed and tested. The new model may be thought of as a generalization of the prototypical Lennard-Jones $(2n,n)$ function, with the form $V(R)=\mathcal{D}_e[1-(R_e/R)^n e^{-\beta(z)z}]^2$, where $z=(R-R_e)/(R+R_e)$ is a dimensionless radial distance variable which approaches 1 as $R\rightarrow\infty$. This form explicitly incorporates the theoretically predicted attractive inverse-power asymptotic behavior $V(R)=\mathcal{D}-C_n/R^n$ associated with most potential energy curves. This ''modified Lennard-Jones'' (MLJ) function is tested against other flexible forms for the potential energy by performing nonlinear least-squares fits both to known numerical potential curves and to spectroscopic line positions. © *2000 American Institute of Physics.* [S0021-9606(00)00909-0]

I. INTRODUCTION

The inversion of experimental data to determine intermolecular potential energy surfaces has long been a central problem in chemical physics. In diatomic molecule spectroscopy the traditional way of doing this has been a two-step approach which involved first a fit of the observed transition frequencies to expressions for level energies as functions of the normal vibrational and rotational quantum numbers, followed by a numerical calculation of the potential function using the RKR (Rydberg–Klein–Rees) method.[1,2] However, the empirical expressions for the level energies used in the first step are usually not constrained to be ''mechanically consistent,'' in that the centrifugal distortion constants are not required to be consistent with the potential energy function defined by the pattern of vibrational energies and inertial rotational constants used to define the RKR potential. In addition, the RKR inversion procedure is based on the first-order semiclassical quantization condition, and hence will not be quantum-mechanically accurate; this can lead to significant discrepancies, particularly for hydrides and other small-reduced-mass molecules. Another difficulty with this approach is that it cannot be directly applied to molecular states with double (or multiple) potential energy minima, cases being encountered with increasing frequency. A more general problem is the fact that this traditional approach cannot readily take account of Born–Oppenheimer breakdown (BOB) effects which give rise to slightly different potential curves for different isotopomers, and to a bond-length dependence of the effective reduced masses associated with molecular rotation and vibration.[3–6]

In response to the difficulties outlined above, recent years have seen increasing use of direct fits of experimental spectroscopic data to analytic potential energy functions, and sometimes more generally to Hamiltonians which combine analytic potential functions with atomic mass dependent radial and centrifugal potential correction functions representing adiabatic and nonadiabatic effects. The earliest work of this type involved the determination of realistic three-dimensional potential energy surfaces for atom–diatom Van der Waals molecules,[7] and this direct-potential-fit approach has seen continuing use in that area. For diatomic molecules most early versions of this approach (called the IPA method) used such fits to determine corrections to RKR potentials determined in the traditional manner.[8,9] Coxon's group later extended that basic approach to combined isotopomer analyses, and was the first to obtain quantitative empirical estimates of adiabatic and nonadiabatic BOB potential correction functions.[10–12] However, since early in this decade a number of groups have been successfully performing direct fits of extensive and highly accurate data sets, often for multiple isotopomers, to fully analytic model potential energy functions, and often also determining the associated BOB radial electronic and centrifugal potential correction functions.[13–20]

A variety of simple analytic functions have been successfully used in direct spectroscopic data fits to represent potential functions for systems with relatively few vibrational levels, or where one type of attractive term (such as the charge-induced dipole attraction in ionic molecules) dominates the interaction.[7,14,18,21–23] However, for chemically bound diatomic molecules with many vibrational levels the problem is distinctly more challenging. In this area some of the most successful functions have been those based on variants of the simple Morse potential with the exponent coefficient being treated as a variable.[15,17,19,20,24–28] However, those models fail to incorporate the theoretically known inverse-power long-range behavior of internuclear diatomic potentials.[29,30] As a result, the potential extrapolation is usually at the mercy of the fitted parameters, rather than being constrained to have the correct theoretically known behavior.

[a]Present and permanent address: Pre-Medicine Program, Intercollege, 46 Makedonitissas Avenue, P.O. Box 4005, Nicosia 1700, Cyprus.
[b]Electronic mail: leroy@UWaterloo.ca

The present paper addresses this problem by introducing a new analytical model for the internuclear potential energy function of a diatomic molecule which has the same flexibility and compactness yielded by the variable-exponent Morse-type potentials, but which can also incorporate the correct theoretically known inverse-power long-range behavior. The new model is described in Sec. II and is tested critically against some other recent models in Sec. III. Section IV then describes a simple extension of the basic model which facilitates avoidance of spurious irregular behavior in the interval between the end of the range spanned by the data and the asymptotic limit.

II. THE BASIC MODIFIED LENNARD-JONES OSCILLATOR MODEL

Like the Morse potential, the prototypical Lennard-Jones $(2n,n)$ function

$$V(R)=\mathcal{D}_e[1-(R_e/R)^n]^2, \tag{1}$$

is a qualitatively correct model for a single minimum diatomic molecule internuclear potential energy function, but does not have the flexibility required to represent accurately extensive experimental information. However, an attractive feature of the Lennard-Jones prototype is the fact that with an appropriate choice of the power n it has the correct theoretically predicted limiting long-range functional behavior. Our efforts at improving this model have concentrated on the generalized form

$$V(R)=\mathcal{D}_e[1-(R_e/R)^n\,\phi(R)]^2, \tag{2}$$

where $\phi(R)$ is an empirical modifying function that may be used to alter the potential to be optimally consistent with experimental data, R_e is the equilibrium bond length and $\mathcal{D}_e$ is the well depth.

The modifying function $\phi(R)$ of Eq. (2) was generated from known RKR or *ab initio* potentials for a variety of systems. For the representative case of the ground electronic state of H_2, whose potential[31] is shown in Fig. 1(A), $\phi(R)$ has the shape shown in Fig. 1(B). Because of its shape and relatively rapid variation with internuclear separation, this function does not lend itself to an efficient representation by a power series expansion, and the same is true for the function $\ln\{\phi(R)\}$. However, if we write $\phi(R)=e^{-\beta_{\rm MLJ}(z)z}$ where $z=(R-R_e)/(R+R_e)$ [one-half of the Ogilvie–Tipping (OT) expansion parameter[32] $z_{\rm OT}(R)$], the exponent parameter $\beta_{\rm MLJ}(z)$ was found to display the much more reasonable behavior seen in Fig. 1(C). In particular, the latter function is everywhere monotonic, is relatively slowly varying on the interval spanning the bowl of the potential well, and it smoothly approaches an asymptote as $V(R)$ approaches the dissociation limit; indeed its only region of moderately strong curvature is at very short distances, far up the repulsive wall. It is clear that this $\beta_{\rm MLJ}(z)$ function would be easy to model in the region where spectroscopic information is available, and its finite limit at large R will facilitate the imposition of long-range constraints. Our resulting proposed ''modified Lennard-Jones oscillator'' (MLJ) potential model is then

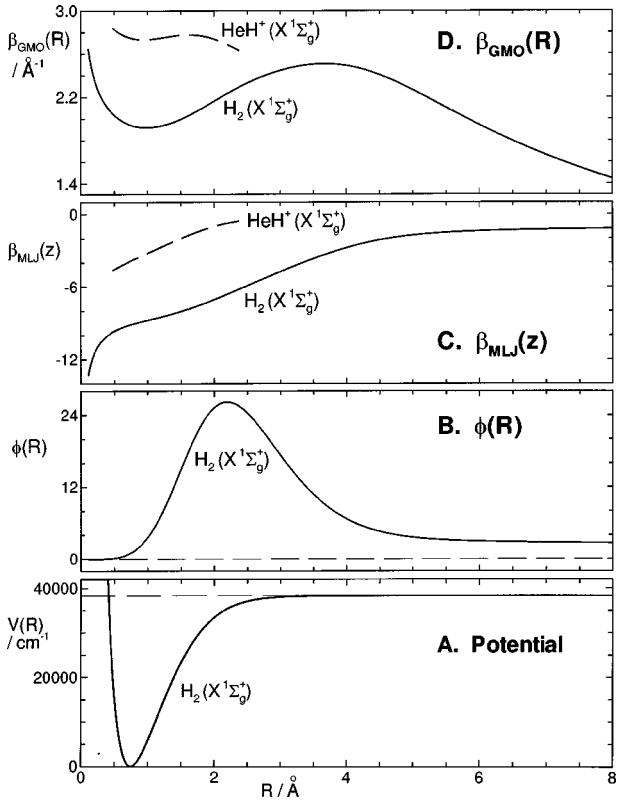

FIG. 1. (A) An *ab initio* potential for ground state H_2; (Ref. 31). (B) The $\phi(R)$ function of Eq. (2) yielded by the H_2 ($X\,^1\Sigma_g^+$) potential of (A); (C) MLJ exponent functions $\beta_{\rm MLJ}(R)$ obtained from the H_2 ($X\,^1\Sigma_g^+$) potential of (A) (solid curve) and the *ab initio* HeH^+ ($X\,^1\Sigma^+$) potential of Ref. 39 using Eq. (3); (D) GMO exponent functions $\beta_{\rm GMO}(R)$ for ground-state H_2 and HeH^+ determined from the *ab initio* potentials of Refs. 31 and 39 using Eq. (11).

$$V(R)=\mathcal{D}_e[1-(R_e/R)^n e^{-\beta_{\rm MLJ}(z)\,z}]^2. \tag{3}$$

In the limit $R\to\infty$, the MLJ potential of Eq. (3) has the form

$$V(R)=\mathcal{D}_e-2\mathcal{D}_e e^{-\beta_\infty}(R_e/R)^n=\mathcal{D}_e-C_n/R^n, \tag{4}$$

where $\beta_\infty\equiv\lim_{R\to\infty}\beta_{\rm MLJ}(z)$, and

$$C_n=2\mathcal{D}_e(R_e)^n e^{-\beta_\infty}\ \text{ or }\ \beta_\infty=\ln[2\mathcal{D}_e(R_e)^n/C_n]. \tag{5}$$

Equation (5) in principle allows either for the empirical determination of C_n or for constraining β_∞ to give a known theoretical C_n value.

The occurrence of β_∞ as a constant in Eqs. (4) and (5) indicates that $\beta_{\rm MLJ}(z)$ must be expressed as a function which will naturally approach a finite limit as $R\to\infty$ (or $z\to1$). The simplest way of doing this is to write it as a power series in z

$$\beta_{\rm MLJ}(z)=\sum_{m=0}^{M}\beta_m z^m, \tag{6}$$

so that

$$\beta_\infty=\lim_{z\to1}\beta_{\rm MLJ}(z)=\sum_{m=0}^{M}\beta_m. \tag{7}$$

The requirement that C_n have an externally determined value may then be imposed by defining the last coefficient of the $\beta(z)$ power series in terms of the others:

$$\beta_M = \ln[2\mathcal{D}_e(R_e)^n/C_n] - \sum_{m=0}^{M-1} \beta_m . \tag{8}$$

This is the form of the MLJ model initially tested below.

III. TESTING THE MODEL

A. Potential forms considered

This section examines four potential energy function models with regard to their general fitting ability, extrapolation properties, flexibility, and compactness. Testing was carried out in two phases: (1) fitting to numerical potentials obtained from *ab initio* calculations or fits to experimental data, and (2) fitting directly to spectroscopic line positions. The four potential functions forms considered here are:

1. The *Ogilvie–Tipping anharmonic oscillator* (OTO)[32,33]

$$V(R) = c_0(z_{\rm OT})^2[1 + c_1 z_{\rm OT} + c_2(z_{\rm OT})^2 + \cdots + c_m(z_{\rm OT})^m], \tag{9}$$

where

$$z_{\rm OT} \equiv 2z = 2(R - R_e)/(R + R_e). \tag{10}$$

2. The *generalized Morse oscillator* (GMO) of Coxon and Hajigeorgiou[15,16,24–26,34,35]

$$V(R) = \mathcal{D}_e[1 - e^{-\beta_{\rm GMO}(R)(R-R_e)}]^2, \tag{11}$$

where

$$\beta_{\rm GMO}(R) = \sum_{m=0} \beta_m^{\rm GMO}(R - R_e)^m. \tag{12}$$

3. The *modified Morse oscillator* (MMO) of Dulick, Bernath, and co-workers[17,27,28]

$$V(R) = \mathcal{D}_e\left[\frac{1 - e^{-\beta_{\rm MMO}(z)z}}{1 - e^{-\beta_\infty^{\rm MMO}}}\right]^2, \tag{13}$$

where

$$\beta_{\rm MMO}(z) = \sum_{m=0} \beta_m^{\rm MMO} z^m \quad \text{and} \quad \beta_\infty^{\rm MMO} = \sum_{m=0} \beta_m . \tag{14}$$

4. The *modified Lennard-Jones oscillator* (MLJ) proposed herein[36]

$$V(R) = \mathcal{D}_e[1 - (R_e/R)^n e^{-\beta_{\rm MLJ}(z)z}]^2 \tag{3}$$

where $\beta_{\rm MLJ}(z)$ is given by Eq. (6).

It is useful to begin with some general comments on features of these different potential forms. The OTO potential is clearly a generalization of the historic Dunham[37,38] power series representation for the potential, with the advantage that use of the reduced variable $z_{\rm OT}$ (whose domain is $[-2, +2]$) means that it avoids the singularities at large–R associated with the conventional Dunham form. However, even though it necessarily goes to a finite asymptote, in the absence of external constraints this form tends to extrapolate quite poorly (see below). Ogilvie did show that with the imposition of algebraic constraint, this form may be required to approach a specified dissociation limit with a specified inverse-power behavior.[33] However, those additional constraints require the introduction of several more high-order power series coefficients than are directly determined by the experimental data set, and the resulting high-power polynomial potential often has spurious nonphysical oscillations in the interval between the region spanned by the data and the $z_{\rm OT} = 2$ $(R = \infty)$ limit.

The GMO potential was the first of the generalized Morse-type models to be successfully applied in direct fits to large bodies of high quality experimental data.[15,16,34,35] However, as illustrated by the comparisons shown in Figs. 1(C) and 1(D), the radial behavior of the $\beta_{\rm GMO}(R)$ function is often more oscillatory and rapidly varying than is the $\beta_{\rm MLJ}(z)$ function defined by the same potential (note that[39] for HeH^+ $R_e = 0.774$ Å). Moreover, while GMO potentials have proved quite effective for accurately representing the potential in the bowl of the potential well, there are problems with its long range behavior. In particular, since $\beta_{\rm GMO}(R)$ is expanded as a simple power series in R, as $R \to \infty$ it necessarily becomes singular. If the highest-power coefficient in the empirically determined $\beta_{\rm GMO}(R)$ expansion happens to be positive, the potential at long range will indeed approach an asymptote, but it will die off there much more rapidly than the theoretically predicted limiting inverse-power behavior. Alternatively, if that highest-power coefficient is negative, instead of smoothly approaching an asymptote at large–R the associated potential will display the type of pathological behavior found for the published[15] ground-state potential for HI plotted in Fig. 2(A); the solid part of the curve indicates the interval spanned by the experimental data used in the analysis, while the dotted region shows how that potential (mis)behaves in the extrapolation region.

The MMO potential form was designed to avoid the sort of pathological behavior seen in Fig. 2(A), and it will indeed always approach a finite asymptote as $R \to \infty$.[17,27,28] However, it will not approach that asymptote with the inverse-power behavior predicted by theory, and there is no guarantee that it will not exhibit irregular behavior in the interval between the region spanned by the experimental data and the asymptote. For example, if the extrapolated $\beta_{\rm MMO}(z)$ at large distances decreases sufficiently rapidly with R, the potential will have a second minimum.

A key feature of the MLJ form is the fact that it can explicitly incorporate the correct theoretically predicted inverse-power asymptotic behavior. However, as with the MMO potential, with $\beta_{\rm MLJ}(z)$ defined by Eq. (6) an MLJ function is not assured of stability beyond the region spanned by the data, and as shown by the dashed curve in Fig. 2(B), rapid decreases of $\beta_{\rm MLJ}(z)$ at large R can give the same sort of spurious outer minima which can occur for the other forms. On the other hand, the straightforward extension of Eq. (6) described in Sec. IV resolves this difficulty, and the resulting potential may be expected to give moderately useful predictions regarding the extrapolation from the highest observed level to dissociation.

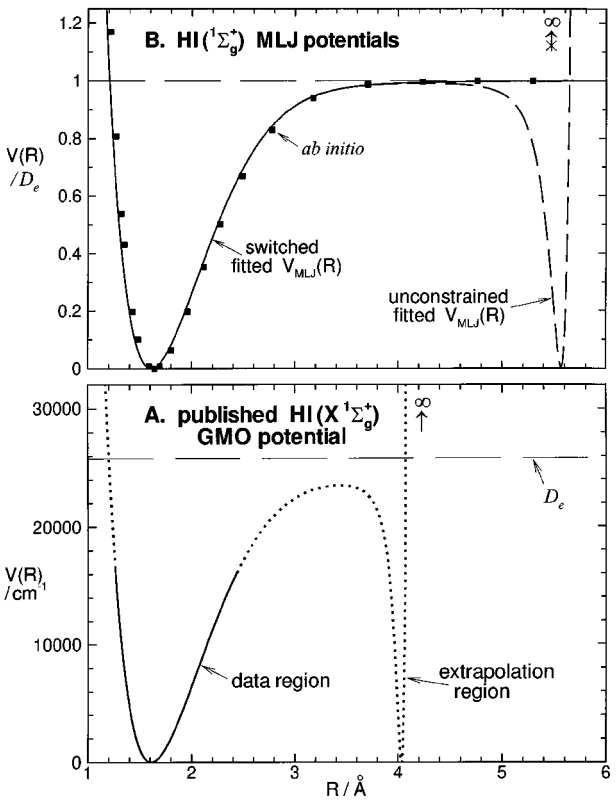

FIG. 2. (A) Published (Ref. 15) GMO potential for ground-state HI showing its pathological behavior (dotted curve segment) beyond the region spanned by the data used in the analysis (solid curve segment). (B) MLJ potentials for HI($X\,^1\Sigma^+$) obtained from fits using the power series $\beta(z)$ of Eq. (6) with no long-range constraints (dashed curve), and from a fit using the switched $\beta^S_{MLJ}(z)$ function of Eq. (15) with C_n fixed at the theoretical value (solid curve), compared with the *ab initio* potential of Ref. 49 (points).

B. Least-squares fitting to numerical potentials

Table I lists the molecular states considered in present tests, and some of their properties. The first set of states (Group A) comprises those for which the tests involved fits to known numerical potential functions, while the second consists of those for which we performed direct fits to sets of experimental transition frequencies. For both sets, n is the power of the asymptotically dominant inverse-power term in the potential, $\mathcal{D}_e$ the well depth, and ''range (% $\mathcal{D}_e$)'' indicates the fraction of the potential well spanned by the numerical potential points used (group A) or the experimental data set (group B).

For each of the six ''Group A'' cases of Table I, the fit to a given potential form was optimized by successively increasing the number of free parameters N until either there was no further reduction in the standard error of the fit σ, or the fit diverged or became unstable when an additional free parameter was introduced. Table II summarizes those results by listing the averages over the six cases of the number of parameters N and standard error σ associated with the optimum fit for each type of model potential. The quantity $\sigma^2 N$ was chosen as an indicator of the overall efficiency of a given model (small values being desirable), as it combines model flexibility, indicated by small σ values, and degree of

TABLE II. Results of fits to numerical potential functions.

A. Fits with $\mathcal{D}_e$ fixed at literature value				
Model	N	σ/cm^{-1}	$\sigma^2 N$	
OTO	12.3($\pm$3.0)	2.59	83	
GMO	9.4($\pm$0.9)	3.40	109	
MMO	8.0($\pm$1.9)	4.11	135	
MLJ	10.3($\pm$1.9)	1.03	11	
B. Fits with $\mathcal{D}_e$ an adjustable parameter				
Model	N	σ/cm^{-1}	$\sigma^2 N$	% err[$\mathcal{D}-V_{max}$]
GMO	8.8($\pm$1.8)	4.23	157	617
MMO	8.7($\pm$2.2)	2.80	68	80
MLJ	10.0($\pm$2.7)	1.09	12	49
C. Fits with $\mathcal{D}_e$ free to points spanning half the well				
Model	N	σ/cm^{-1}	$\sigma^2 N$	% err[$\mathcal{D}-V_{max}$]
GMO	7.7($\pm$2.2)	0.088	0.059	162[a]
MMO	7.5($\pm$0.8)	0.146	0.159	93[a]
MLJ	8.5($\pm$2.3)	0.073	0.045	147[a]

[a]Average of the best five extrapolations.

TABLE I. Species employed in testing the analytical potential models, and some of their properties. The ''range (% $\mathcal{D}_e$)'' column indicates the fraction of the potential well spanned by the data used in the fits.

A. Fits to numerical potential functions					
Species	n	$\mathcal{D}_e$/cm^{-1}	Range (% $\mathcal{D}_e$)	Type	Ref.
CO ($X\,^1\Sigma^+$)	5	90 670.	70.0	RKR	34
HCl ($X\,^1\Sigma^+$)	6	37 100.	96.0	IPA	26
HF ($X\,^1\Sigma^+$)	6	49 362.	99.0	IPA	12
Cs_2 ($X\,^1\Sigma^+$)	6	36 49.5	99.24	IPA	59
I_2 ($X\,^1\Sigma^+$)	6	12 544.	99.80	RKR[a]	60
H_2 ($X\,^1\Sigma^+$)	6	38 292.8	99.9985	*ab initio*	31

B . Fits to spectroscopic line positions						
Species	n	$\mathcal{D}_e$/cm^{-1}	Range (% $\mathcal{D}_e$)	Isotopomers	# data	Ref.
HCl ($X\,^1\Sigma^+$)	6	37 100.	96	H ^{35}Cl	2673	26
HI ($X\,^1\Sigma^+$)	6	25 778.	62	HI & DI	560	15
AlH ($X\,^1\Sigma^+$)	6	24 600.	48	AlH & AlD	732	27
AlCl ($X\,^1\Sigma^+$)	6	41 296.	26	Al ^{35}Cl&Al ^{37}Cl	2299	17

[a]RKR potential calculated from the constants of Ref. 60.

compactness, indicated by small N values. The variance σ^2 is used instead of the standard error to reflect our preference for assigning more importance to the ability of a specific model to achieve a good fit, even at the expense of a slightly greater number of parameters. According to this criterion, the MLJ potential is clearly the best of the model functions considered here.

This phase of the testing was performed with $\mathcal{D}_e$ being either fixed at the accepted literature value (part A of Table II), or treated an adjustable parameter (part B of Table II). It is interesting to note that the increased flexibility introduced by freeing $\mathcal{D}_e$ sometimes even allows the total number of free parameters to be reduced. The accuracy with which $\mathcal{D}_e$ may be expected to be determined in such fits is of course expected to depend on the energy gap between the dissociation limit $\mathcal{D}$ and the longest-range potential point used in the analysis $V_{\max}$. As a test of this extrapolation ability, the last column of Table IIB lists the average (over the six cases) values of the percent error in the prediction of the gap between $V_{\max}$ and $\mathcal{D}$, and Table IIC shows analogous results for the case in which the data sets used were truncated to points spanning only the lower half of the potential well. On the basis of this criterion, the MLJ model is again superior to the others (the OTO model was not included in this set of comparisons because it does not naturally approach an asymptote and does not contain $\mathcal{D}_e$ as an adjustable parameter). However, *none* of them, including the unconstrained (see below) MLJ potential form of Eqs. (3) and (6), inspires confidence with regard to its ability to extrapolate to determine reliable $\mathcal{D}_e$ values.

In summary, in fits to numerical potentials the MLJ potential form performs at least as well as, and usually much better than do the other models considered here. We should point out that in the above fits, all numerical potential function values were weighted equally; while not ideal, this could not be helped.[40–42] However, we doubt that this biases our conclusions, and we can anecdotally report that there was no systematic variation in goodness of fit between the inner and outer limbs of the potential. In any case, while the above fits to numerical potentials are an appropriate starting point for this study, the more critical test is the capability of the various potential models in direct fits to real experimental data, presented below.

C. Least-squares fitting to spectroscopic line positions

The computational method employed here for fitting potential functions to spectroscopic data is essentially the same as the ''direct potential fit'' (DPF) procedure described by Coxon and Hajigeorgiou[15] and applied by a number of other groups.[7,13,14,17,18,20,23] It involves numerically solving the Schrödinger equation for each eigenstate involved in the set of experimental transitions, and using the Hellmann–Feynman theorem to generate from the resulting radial eigenfunctions the partial derivatives required for the nonlinear least-squares procedure. As well as determining the electronic potential energy function, this procedure may use high–J data and combined isotopomer analyses to determine BOB correction functions.

TABLE III. Results of direct fitting of spectroscopic data to analytic potential functions.

Model	N	$\overline{\sigma_f}$	$\overline{\sigma_f^2}\,N$
OTO	9.8($\pm$3.6)	0.889	6.79
GMO	8.5($\pm$3.1)	0.894	7.70
MMO	7.7($\pm$2.9)[a]	1.525	17.8
MLJ	10.8($\pm$1.9)	0.88	8.2

[a]We were unable to obtain a stable MMO potential to the full data set for $H^{35}Cl$, so this N value is an average over three cases.

The four molecular states considered in this phase of the model testing are listed in Table I; the input spectroscopic data were the same as those used in the analyses published in the indicated references. For HI, AlCl, and AlH we performed the same type of combined isotopomer analysis reported previously,[15,17,27] while for HCl only the dominant isotopomer $H^{35}Cl$ was considered. This last case is of particular interest since the available data for this isotopomer include vibrational levels spanning 96% of the potential well, as well as quasibound rotational states which should be especially sensitive to behavior of the potential near dissociation. In view of the poor reliability of potential fits in determining $\mathcal{D}_e$ (see Table II), in all of our fits to experimental data $\mathcal{D}_e$ was held fixed at the best known experimental value.

Table III summarizes the results of these fits. Again, N is the average (over the four cases) number of adjustable parameters in the potential function (additional parameters characterizing Born–Oppenheimer breakdown behavior are not included in this sum). In this case, $\overline{\sigma_f}$ is the average dimensionless standard deviation of the fits; for a given fit a value of $\overline{\sigma_f}$ near unity indicates that on average the data are represented by the model within their estimated uncertainties.[43] These results indicate clearly that there is no appreciable difference between the various models, all of which perform equally well in representing the spectroscopic data. However, we were unable to obtain a stable MMO fit to $H^{35}Cl$ when the data spanned more than 50% of $\mathcal{D}_e$. In general, the MMO model appears to be less flexible than all the others, which is a definite disadvantage; on the other hand this could be considered an advantage in fitting low-v data, in that systematic error in spectroscopic data will not be disguised by inclusion of unsupported or superfluous parameters.

From this point on attention is focused on the properties of the MLJ model, since it is as good as or better than the other forms considered for practical representation of known potential points or raw spectroscopic data, and it has the added advantage of being able to incorporate the correct theoretically predicted long-range behavior. Figure 3(A) compares the MLJ potential for AlH (solid curve) with a recent *ab initio* potential[44] for this system. Although the spectroscopic data used to define this potential span only approximately half the well depth, there is clearly quite good agreement in the extrapolation region.

As another test case, a fit was carried out using a subset of the $H^{35}Cl$ data set consisting of transitions involving levels spanning only the lower half of the potential well. In Fig.

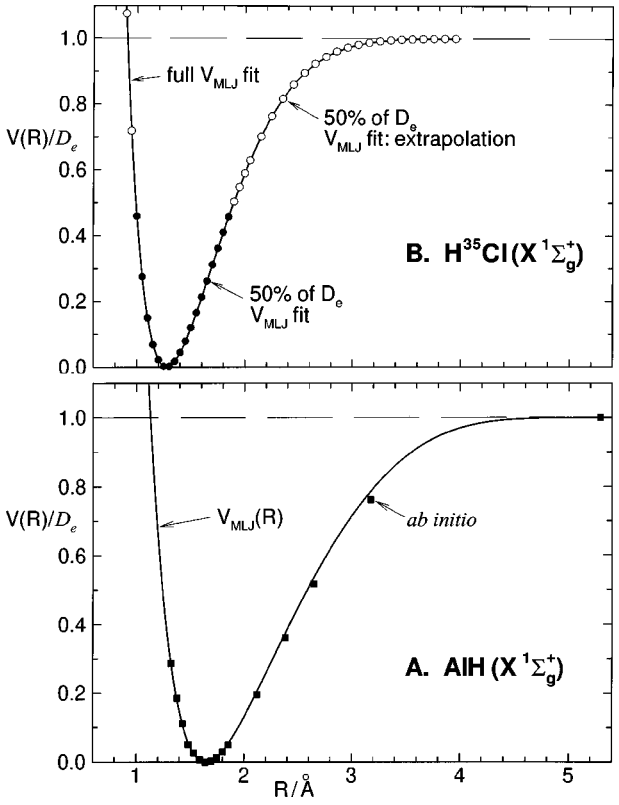

FIG. 3. (A) MLJ potential for AlH ($X\,^1\Sigma^+$) obtained from a direct fit to the spectroscopic data of Ref. 27, compared to the *ab initio* points from Ref. 44. (B) MLJ potentials for $H^{35}Cl$ ($X\,^1\Sigma^+$) obtained a direct fit to the complete data set spanning 96% of the well (solid curve), and that yielded by a fit to data for the lower 50% of the well (points: Solid points in data region and open points in extrapolation region).

3(B) the resulting MLJ potential is shown as solid points on the interval spanned by the data and open points in the extrapolation region, while the solid curve is the MLJ potential obtained from a fit to the complete data set (including vibrational levels spanning 96% of the well); the agreement in the extrapolation region is remarkably good.

It turns out, however, that the stability of the $H^{35}Cl$ extrapolation shown by the open points in Fig. 3(B) rests on the fortuitous fact that the fitted $\beta_{\rm MLJ}(z)$ function for that case does *not* accidentally drop off steeply or become large and negative in the region beyond that spanned by the data set used (spanning the lower half of the potential well). Unfortunately, the latter is what happened with the ''unconstrained'' MLJ potential obtained from a fit to the data for HI shown as a dashed curve in Fig. 2(B), this gave rise to the same sort of pathological behavior found for the GMO potential seen in Fig. 2(A). Although the MLJ function does not become singular and eventually drops back to the asymptote as $R\to\infty$ (while the GMO function $\to\infty$), its behavior in the extrapolation region is clearly unacceptable. The following section, therefore, presents a means of ensuring stable long-range behavior by introducing constraints on $\beta_{\rm MLJ}(z)$ in the extrapolation region.

IV. IMPROVED LONG-RANGE CONSTRAINT

As shown by the dashed curve in Fig. 2(B), in its basic form the MLJ model can display anomalous behavior in the interval between the region spanned by the experimental data and the dissociation limit. One approach to addressing this problem would be to use Eq. (8) to impose the requirement that the potential approach the limit with the correct $\mathcal{D}_e - C_n/R^n$ behavior, with the value of C_n being held fixed at a realistic theoretically predicted value. Unfortunately, this additional constraint is often not sufficiently strong to achieve the desired result. In particular, the subtle functional behavior of $\beta_{\rm MLJ}(z)$ required to model the data accurately often requires this function to be represented by a relatively high-order polynomial in z, and high-order polynomials are notoriously unstable for extrapolation, even when constrained to match a specified value [such as β_∞ of Eq. (5)] at the outer end of the range. What often happens in practice, is that the fitted $\beta_{\rm MLJ}(z)$ polynomial varies very smoothly and gradually across the region spanned by the data, and then has a spurious extremum between that region and the end of the range where it attains the limiting value imposed by Eq. (8). Moreover, imposing the additional constraint that $\beta_{\rm MLJ}(z)$ have zero slope at $z=1$ ($R\to\infty$) did not improve the situation. It is obvious, then, that use of Eq. (8) is not an adequate means of imposing stable extrapolation behavior on $\beta_{\rm MLJ}(z)$.

One approach to the above problem would be to represent $\beta_{\rm MLJ}(z)$ by a more sophisticated analytic function which does not have the tendency to extrapolate badly associated with simple polynomials, such as a rational polynomial (ratio of polynomials) or a Fourier series. However, the resulting complexity of form would tend to intimidate some potential users and would make the least-squares fitting to data more difficult to implement. Instead, the approach (successfully) adopted here was to retain the basic z–polynomial representation of $\beta_{\rm MLJ}(z)$, but to modify it by introducing a switching function which damps the polynomial beyond the range of the data and causes $\beta_{\rm MLJ}(z)$ to smoothly approach the specified β_∞ limit of Eq. (5) without spurious intervening irregularities

$$\beta^S_{\rm MLJ}(z) = f_S(R)\left[\sum_{m=0} \beta_m z^m - \beta_\infty\right] + \beta_\infty . \tag{15}$$

The switching function used here is

$$f_S(R) = 1/[\,e^{\alpha_S (R-R_S)} + 1\,], \tag{16}$$

where α_S is a damping strength parameter and R_S is the distance where the damping is half-complete. This function is everywhere continuous, has values ranging from unity to zero as R increases, and rapidly drops off at distances significantly past R_S, providing for a smooth transition from a polynomial representation of at short distances to the asymptotic value β_∞.

Since this switching function is introduced in order to damp an otherwise runaway polynomial function beyond the range of the data, it makes sense to choose R_S to lie near the outermost classical turning point sampled by the data, $R_{\rm max}$; in practice, setting R_S slightly larger than $R_{\rm max}$ (say, by 0.5 Å) seems to work well. However, choosing a value for the exponent damping coefficient α_S, which controls the abruptness of the switching, is somewhat more arbitrary. One plausible approach would be to give it a value such as

$4/(R_S-R_e)$, so that the polynomial part of $\beta^S_{\mathrm{MLJ}}(z)$ would dominate (by ~98%) near the potential minimum. An alternate view is that α_S should increase with (R_S-R_e), in order to ensure that the polynomial part of $\beta^S_{\mathrm{MLJ}}(z)$ would be rapidly damped past R_S. While a variety of such rules were tried, there seemed to be no single definition of α_S which would work well in all cases. This might have been expected, however, since the degree of polynomial blowup which has to be accounted for would differ markedly from one case to another. In any case, the particular choice of α_S is not critical.

In principle both α_S and R_S could be treated as additional fitting parameters, and this has been done in some applications of this model.[45] However, since the essential objective of introducing the switching function is to deal with unacceptable functional behavior on the interval *beyond* the range of the data, it may be somewhat questionable to attempt to determine that function from the data themselves. It seems to us more reasonable (as well as more convenient) to fix these parameters at plausible conveniently rounded values, which can be modified as demanded by the particular anomalous behavior we are trying to suppress,[46] and to allow the polynomial coefficients to be responsible for the way $\beta^S_{\mathrm{MLJ}}(z)$ accommodates the data.

Our first test of the switching function approach is its application to the ground state of HI, for which pathological behavior was found in both the fitted GMO potential of Ref. 15 [see Fig. 2(A)] and in a fitted MLJ potential based on the simple polynomial $\beta(z)$ function of Eq. (6). For this case long-range potential theory shows that the power n in Eq. (3) should be 6,[29] while the London formula yields a realistic estimate of $C_6=2.55\times10^5\,\mathrm{cm}^{-1}\,\text{Å}^6$ from the known[47] atomic polarizabilities and ionization potentials.[48] The dashed curve in Fig. 2(B) was obtained by fitting data spanning 62% of the potential well to an MLJ potential in which $\beta_{\mathrm{MLJ}}(z)$ had the simple polynomial form of Eq. (6). In contrast, an equally good fit of those same data to an MLJ potential using the switched $\beta^S_{\mathrm{MLJ}}(z)$ function of Eq. (15) with $\alpha_S=1.55\,\text{Å}^{-1}$ and $R_S=3.11$ Å gives the potential shown as a solid curve in Fig. 2(B). The latter is clearly very well-behaved at long range, and is in excellent qualitative agreement with a reported *ab initio* potential.[49]

A second application of this approach was to the ground state of H_2, for which an accurate modern *ab initio* potential extends from 0.1 to 9.5 Å.[31] Potential energies up to 75% of $\mathcal{D}_e$, corresponding to the radial range 0.44–1.72 Å, were fitted to an MLJ function for which the switching function in $\beta^S_{\mathrm{MLJ}}(z)$ is characterized by parameters $\alpha_S=1.11\,\text{Å}^{-1}$ and $R_S=2.22$ Å. For this case again $n=6$ and an accurate $C_6=3.132\times10^4\,\mathrm{cm}^{-1}\,\text{Å}^6$ known from theory[29] was used to define β_∞. In Fig. 4 the solid points are values of $\beta_{\mathrm{MLJ}}(R)$ [defined by Eq. (3) and the *ab initio* potential] on the interval spanning the lower 75% of the well, the open points are the analogous values in the longer and shorter range regions, and the solid curve is the switched $\beta^S_{\mathrm{MLJ}}(z)$ function determined from a fit to the solid points. The agreement is clearly quite reasonable over the entire range, and the stability of the extrapolation is demonstrated convincingly.

Our final illustrative application considers the ground state of HF, for which $\beta_{\mathrm{MLJ}}(z)$ values generated from Eq. (3) and the published potential of Ref. 50 are shown as round points in the lower half of Fig. 5; the points are solid on the interval spanned by the inner and outer turning points of the experimental data used in the analysis, and are open points in the extrapolation region beyond $R_{\max}=2.87$ Å. For this case $n=6$ and the theoretical value[50] $C_6=3.743\times10^4\,\mathrm{cm}^{-1}\,\text{Å}^6$

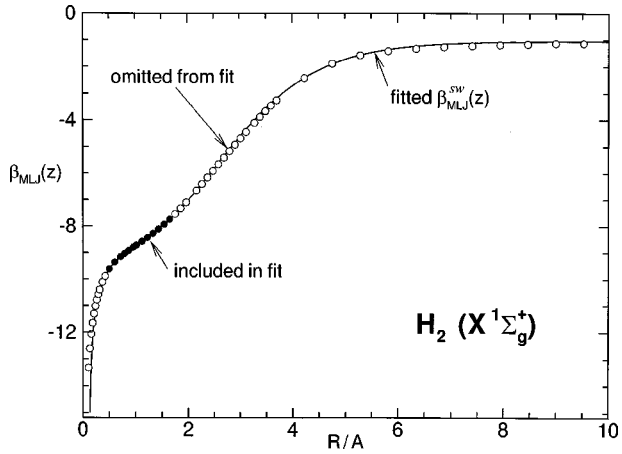

FIG. 4. $\beta_{\mathrm{MLJ}}(R)$ function for the $X\,^1\Sigma_g^+$ state H_2 (solid curve) obtained from a fit to values (solid points) generated from Eq. (15) and the *ab initio* potential of Ref. 31; the open points also generated from the *ab initio* potential were not included in the fit.

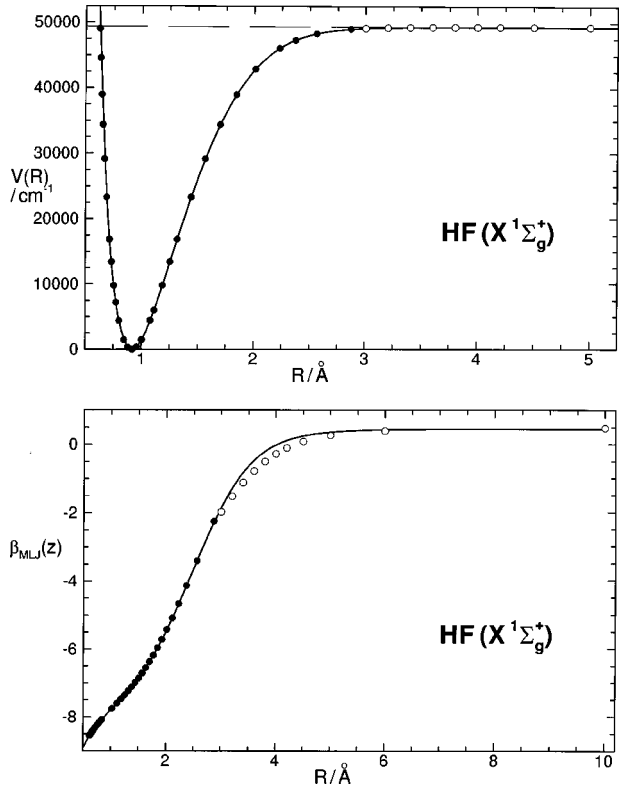

FIG. 5. *Lower segment:* For HF($X\,^1\Sigma_g^+$), comparison of $\beta_{\mathrm{MLJ}}(R)$ values generated from Eq. (3) and the potential of Ref. 50 in the experimental data (solid points) and long-range (open points) regions, with a fitted $\beta^S_{\mathrm{MLJ}}(z)$ with C_n fixed at the theoretical value. *Upper segment:* Comparison of the resulting switched-MLJ potential (solid curve) with the potential of Ref. 50 (points).

defines $\beta_\infty = 0.449$. A fit of Eq. (15) with $\alpha_S = 1.68\,\text{Å}^{-1}$ and $R_S = 3.37$ Å to the solid points for $R \leqslant R_{\max} = 2.87$ Å yielded the solid curve seen in the lower half of Fig. 5, while the resulting ''switched MLJ potential'' (points) is compared with the full published potential[50] in the upper half of Fig. 5. This comparison shows that the $\beta_{\text{MLJ}}(R)$ match is nearly perfect in the region spanned by the experimental data, deviates slightly in the region 3–5 Å, then regains its agreement at larger R. Close inspection of the $\beta_{\text{MLJ}}(z)$ function calculated from the Zemke *et al.* potential[50] shows that there is a discontinuity in slope at the join ($R_{\max} \approx 2.87$ Å) between the experimental curve and the purely theoretical long-range section. This likely reflects uncertainties in the calculated C_8 and C_{10} constants or long-range exchange interaction,[50] and/or the neglect of damping in the analytic model for the long-range potential. In any case, β-switched potential shown by the solid curve in the lower segment of Fig. 5 is free of instabilities or irregularities, and approaches dissociation in accord with the theoretical C_6 estimate used to define our β_∞ value.[50]

For the initial test fits shown in Table II, the inverse-power form of the potential tail was introduced by the analytic form of the MLJ function, but the value of the associated [see Eq. (5)] C_n or β_∞ value was not held fixed. However, on repeating those fits using the switched $\beta^S_{\text{MLJ}}(z)$ function of Eq. (15) with C_n fixed and $\mathcal{D}_e$ treated as a free parameter, the average error in the extrapolation to determine $\mathcal{D}_e$, ''%error$[\mathcal{D} - V_{\max}]$'' in Table II, decreased by almost a factor of 2, to 27%. While this is significantly higher than the 5–10% error typically associated with near-dissociation expansion vibrational extrapolations,[51,52] it is substantially better than the extrapolations attained using other types of model potential functions which do not incorporate correct asymptotic behavior.

V. DISCUSSION AND CONCLUSIONS

The present work has introduced the generalized MLJ potential function of Eq. (3), which asymptotically attains the theoretically expected limiting long-range behavior $V(R) = \mathcal{D} - C_n/R^n$. It was shown that with $C_n = 2\,\mathcal{D}_e\,(R_e)^n\,e^{-\beta_\infty}$ unconstrained, this function performed as well as or better than three other analytic potentials introduced in recent years with respect to general fitting ability, extrapolation properties, flexibility, and compactness. Moreover, when C_n is constrained to have a realistic theoretical value, and (if necessary) accidental spurious long-range behavior of the exponent function $\beta_{\text{MLJ}}(z)$ constrained through use of a switching function, its extrapolation properties improve markedly. Since its preliminary introduction in 1994,[36] the advantages of this form have already led to its adoption in a number of practical data analyses.[45,53–55]

The present results suggest, therefore, that although they serve equally well for representing data, their inappropriate and sometimes pathological long-range behavior make the GMO potential of Eq. (11) and MMO potential of Eq. (13) distinctly less appropriate than the MLJ function as realistic overall models for potential energy functions. Moreover, our experience suggests that obtaining stable fits to the MMO

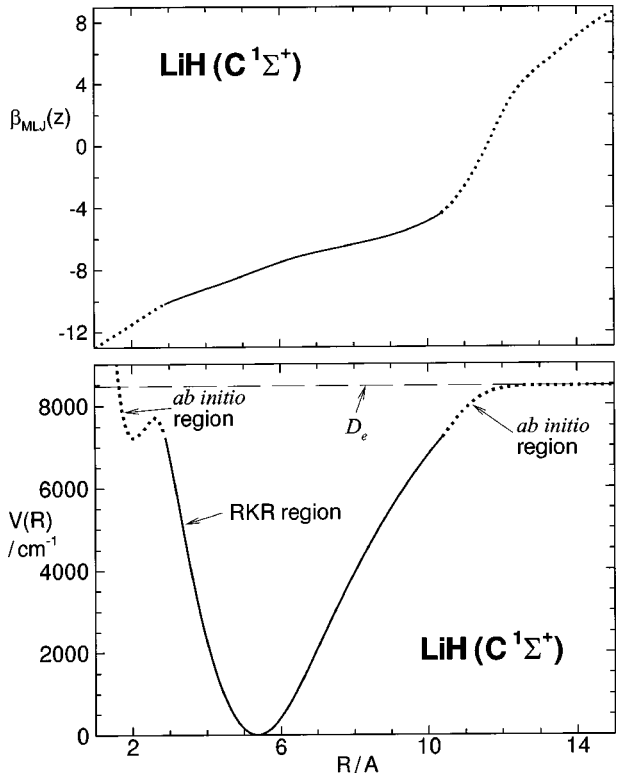

FIG. 6. *Lower segment:* Recommended composite LiH($C\,^1\Sigma^+$) potential of Ref. 57. *Upper segment:* $\beta_{\text{MLJ}}(R)$ function determined from this LiH potential and Eq. (3).

form is sometimes more difficult than for the others. Similarly, while the OTO potential of Eq. (9) also gives excellent fits to data and can be constrained to approach a specified dissociation limit with desired inverse-power behavior,[33] the requisite constraints are fairly complex and require the addition of several more high-power terms in the expansion that are required by the data, which in turn substantially increases the proclivity for spurious nonphysical behavior at large–R. The generalized potential energy function (GPEF) function of Šurkus, which has been successfully used for a number of data analyses, can also be constrained to attain the correct long-range behavior.[18,56] However, in an application to He H^+, Coxon and Hajigeorgiou found this form to be somewhat inflexible when applied to data extending all the way to dissociation.[45] Thus, the generalized MLJ form presented here seems to have substantial advantages over the other potential function models considered herein.

In the course of this work a number of variants of the MLJ form were examined in which the exponent function was written more generally as $e^{-\beta(\zeta_1)\,\zeta_1}$, where ζ_1 and ζ_2 are alternate choices for the distance expansion variable. However, the ability of the long-range tail of this potential to take on the expected inverse-power long-range form with a specified C_n coefficient places considerable limitations on these choices, and in practice the choice $\zeta_1 = \zeta_2 = z \equiv (R - R_e)/(R + R_e)$ of Eq. (3) was found to be the most effective.

The final point we wish to raise is the fact that a property of the MLJ potential form which initially seems to be only a potential source of problems is actually one of its attractive features. In particular, the dashed curve in Fig. 2(B) shows

that if $\beta_{\mathrm{MLJ}}(R)$ at large R decreases more rapidly than z increases, the function may give rise to a potential with a spurious additional minimum. The fact that this particular potential continues past that minimum to show a steep potential wall before asymptotically approaching $V(R)/\mathcal{D}_e=1$ reflects the fact that the unconstrained extrapolated $\beta_{\mathrm{MLJ}}(z)$ function grows to a large negative value at the $z=1$ limit. We have seen (in Sec. IV) that such pathological behavior can be readily controlled by use of a switching function. However, this behavior also indicates that the MLJ functional form could accurately describe potential functions for ''shelf'' or double minimum states! As an illustration of this point, the lower half of Fig. 6 shows a double minimum potential recently determined for the $C\,^1\Sigma^+$ state of LiH by combining an RKR potential for the main well region (solid curve segment) with *ab initio* points for shorter and longer range (dotted curve segments).[57] The upper half of Fig. 6 shows the $\beta_{\mathrm{MLJ}}(z)$ function determined from this potential using Eq. (3). It is remarkable to see that $\beta_{\mathrm{MLJ}}(z)$ shows no substantial irregular behavior in the neighborhood of the shallow second inner well! Indeed, its most marked ''irregularity'' is the marked change in slope near $R=10$ Å, which is almost certainly due to an avoided crossing with the $D\,^1\Sigma^+$ state.[58] Thus, not only does the MLJ form readily account for the second inner well, but its behavior also provides an indication of the presence of an avoided crossing. A direct fit of the new LiH($C\,^1\Sigma^+$) data[57] involving levels lying both below and above the barrier maximum seen in Fig. 6, and applications to other shelf and double minimum states are currently under way.[46]

ACKNOWLEDGMENTS

We are pleased to acknowledge helpful discussions with Professor J. A. Coxon, Professor P. F. Bernath, and Mr. J. Y. Seto. This research was supported by the Natural Sciences and Engineering Research Council of Canada.

[1] (a) R. Rydberg, Z. Phys. **73**, 376 (1931); (b) O. Klein, *ibid.* **76**, 226 (1932); (c) R. Rydberg, *ibid.* **80**, 514 (1933); (d) A. L. G. Rees, Proc. Phys. Soc. (London) **59**, 998 (1947).
[2] M. S. Child, *Semiclassical Mechanics with Molecular Applications* (Clarendon, Oxford, 1991).
[3] R. M. Herman and A. Asgharian, J. Mol. Spectrosc. **19**, 305 (1966).
[4] P. R. Bunker and R. E. Moss, Mol. Phys. **33**, 417 (1977).
[5] J. K. G. Watson, J. Mol. Spectrosc. **80**, 411 (1980).
[6] R. M. Herman and J. F. Ogilvie, Adv. Chem. Phys. **103**, 187 (1998).
[7] R. J. Le Roy and J. van Kranendonk, J. Chem. Phys. **61**, 4750 (1974).
[8] W. M. Kosman and J. Hinze, J. Mol. Spectrosc. **56**, 93 (1975).
[9] C. R. Vidal and H. Scheingraber, J. Mol. Spectrosc. **65**, 46 (1977).
[10] J. A. Coxon, J. Mol. Spectrosc. **117**, 361 (1986).
[11] J. A. Coxon, J. Mol. Spectrosc. **133**, 96 (1989).
[12] J. A. Coxon and P. G. Hajigeorgiou, J. Mol. Spectrosc. **142**, 254 (1990).
[13] M. Gruebele, Mol. Phys. **69**, 475 (1990).
[14] R. Brühl, J. Kapetanakis, and D. Zimmermann, J. Chem. Phys. **94**, 5865 (1991).
[15] J. A. Coxon and P. G. Hajigeorgiou, J. Mol. Spectrosc. **150**, 1 (1991).
[16] J. A. Coxon, J. Mol. Spectrosc. **152**, 274 (1992).
[17] H. G. Hedderich, M. Dulick, and P. F. Bernath, J. Chem. Phys. **99**, 8363 (1993).
[18] A. Šurkus, Chem. Phys. Lett. **279**, 236 (1997).
[19] E. G. Lee, J. Y. Seto, T. Hirao, P. F. Bernath, and R. J. Le Roy, J. Mol. Spectrosc. **194**, 197 (1999).
[20] J. Y. Seto, Z. Morbi, F. Charron, S. K. Lee, P. F. Bernath, and R. J. Le Roy, J. Chem. Phys. **110**, 11756 (1999).
[21] R. J. Le Roy, J. S. Carley, and J. E. Grabenstetter, Faraday Discuss. Chem. Soc. (London) **62**, 169 (1977).
[22] R. J. Le Roy and J. M. Hutson, J. Chem. Phys. **1987**, 827 (1987).
[23] J. Tellinghuisen, J. Mol. Spectrosc. **173**, 223 (1995).
[24] P. J. Kuntz and A. C. Roach, J. Chem. Soc. Faraday Trans. II **68**, 259 (1972).
[25] R. J. Duchovic and W. L. Hase, Chem. Phys. Lett. **110**, 474 (1984).
[26] J. A. Coxon and P. G. Hajigeorgiou, J. Mol. Spectrosc. **139**, 84 (1990).
[27] J. B. White, M. Dulick, and P. F. Bernath, J. Chem. Phys. **99**, 8371 (1993).
[28] J. M. Campbell, M. Dulick, D. Klapstein, J. B. White, and P. F. Bernath, J. Chem. Phys. **99**, 8379 (1993).
[29] J. O. Hirschfelder and W. J. Meath, in *Intermolecular Forces*, Vol. 12 of *Adv. Chem. Phys.*, edited by J. O. Hirschfelder (Interscience, New York, 1967), pp. 3–106.
[30] R. J. Le Roy, in *Molecular Spectroscopy*, edited by R. Barrow (Chemical Society of London, London, 1973), Vol. 1, Specialist Periodical Report 3, pp. 113–176.
[31] W. Kołos, K. Szalewicz, and H. J. Monkhorst, J. Chem. Phys. **84**, 3278 (1986).
[32] J. F. Ogilvie, Proc. R. Soc. (London), Ser. A **378**, 287 (1981).
[33] J. F. Ogilvie, J. Chem. Phys. **88**, 2804 (1988).
[34] J. A. Coxon and P. G. Hajigeorgiou, Can. J. **94**, 40 (1992).
[35] J. A. Coxon and P. G. Hajigeorgiou, Chem. Phys. **167**, 327 (1992).
[36] P. G. Hajigeorgiou and R. J. Le Roy, in *49th Ohio State University International Symposium on Molecular Spectroscopy*, Columbus, Ohio (1994), paper WE04.
[37] J. L. Dunham, Phys. Rev. **41**, 713 (1932).
[38] J. L. Dunham, Phys. Rev. **41**, 721 (1932).
[39] D. M. Bishop and L. M. Cheung, J. Mol. Spectrosc. **75**, 462 (1979).
[40] It would of course have been better to perform weighted fits, since different points on empirical or *ab initio* potentials may be expected to have different uncertainties. However, while the uncertainties in RKR turning points due to the uncertainties in the molecular constants determining them can be calculated (Ref. 41), and the calculation of uncertainties in fitted analytic potentials (or IPA potential correction functions) is quite straightforward (Ref. 42), these methods have seen almost no use in practice (except in Ref. 42). Thus, without repeating the data analyses which yielded the potentials used herein, proper unequal weights could not be obtained.
[41] J. Tellinghuisen, J. Mol. Spectrosc. **141**, 258 (1990).
[42] C. E. Chuaqui, R. J. Le Roy, and A. R. W. McKellar, J. Chem. Phys. **101**, 39 (1994).
[43] R. J. Le Roy, J. Mol. Spectrosc. **191**, 223 (1998).
[44] J. M. O. Matos, P.-A. Malmqvist, and B. O. Roos, J. Chem. Phys. **86**, 5032 (1987).
[45] J. A. Coxon and P. G. Hajigeorgiou, J. Mol. Spectrosc. **193**, 306 (1999).
[46] J. Y. Seto, M.Sc. Thesis, Department of Chemistry, University of Waterloo (2000).
[47] D. R. Lide, Editor, *Handbook of Chemistry and Physics* (CRC, Ann Arbor, MI, 1993).
[48] G. C. Maitland, M. Rigby, E. B. Smith, and W. A. Wakeham, *Intermolecular Forces - Their Origin and Determination* (Oxford University Press, Oxford, UK, 1981).
[49] H.-J. Werner, E.-A. Reinsch, and P. Rosmus, Chem. Phys. Lett. **78**, 311 (1981).
[50] W. T. Zemke, W. C. Stwalley, J. A. Coxon, and P. G. Hajigeorgiou, Chem. Phys. Lett. **177**, 412 (1991).
[51] R. J. Le Roy and W.-H. Lam, Chem. Phys. Lett. **71**, 544 (1980).
[52] R. J. Le Roy, J. Chem. Phys. **101**, 10217 (1994).
[53] J. A. Coxon and P. G. Hajigeorgiou, in *49th Ohio State University International Symposium on Molecular Spectroscopy*, Columbus, Ohio (1994), paper WE05.
[54] J.-U. Grabow, A. S. Pine, G. T. Fraser, F. J. Lovas, and R. D. Suenram, J. Chem. Phys. **102**, 1181 (1995).
[55] J. A. Coxon and R. Colin, J. Mol. Spectrosc. **181**, 215 (1997).
[56] A. A. Šurkus, R. J. Rakauskas, and A. B. Bolotin, Chem. Phys. Lett. **105**, 291 (1984).
[57] J.-J. Chen, W.-T. Luh, and G. H. Jeung, J. Chem. Phys. **110**, 4402 (1999).
[58] A. Boutalib and F. X. Gadéa, J. Chem. Phys. **97**, 1144 (1992).
[59] W. Weickenmeier, U. Deimer, M. Wahl, M. Raab, W. Demtröder, and W. Müller, J. Chem. Phys. **82**, 5354 (1985).
[60] S. Gerstenkorn and P. Luc, J. Phys. (France) **46**, 867 (1985).